A COUPLED STRUCTURAL-MAGNETIC STRAIN AND STRESS MODEL FOR MAGNETOSTRICTIVE TRANSDUCERS

Marcelo J. Dapino[1], Ralph C. Smith[2], LeAnn E. Faidley[3] and Alison B. Flatau[4]

[1] (Correspondence)
Department of Aerospace Engineering
and Engineering Mechanics
Iowa State University
2019 Black Engineering Building
Ames, IA 50011
E-mail: marcelod@iastate.edu
Phone: (515) 294-0084

[2] Center for Research in Scientific Computation
Department of Mathematics
North Carolina State University
Raleigh, NC 27695

[3,4] Department of Aerospace Engineering
and Engineering Mechanics
Iowa State University
Ames, IA 50011

Abstract

This paper addresses the modeling of strains and forces generated by magnetostrictive transducers in response to applied magnetic fields. The magnetostrictive effect is modeled by considering both the rotation of magnetic moments in response to the field and the elastic vibrations in the transducer. The former is modeled with the Jiles-Atherton model of ferromagnetic hysteresis in combination with a quartic magnetostriction law. The latter is modeled through force balancing which yields a PDE system with magnetostrictive inputs and boundary conditions given by the specific transducer design. The solution to this system provides both rod displacements and forces. The calculated forces are used to quantify the magnetomechanical effect in the transducer core, i.e., the stress-induced magnetization changes. This is done by considering a 'law of approach' to the anhysteretic magnetization. The resulting model provides a representation of the bidirectional coupling between the magnetic and elastic states. It is demonstrated that the model accurately characterizes the magnetic hysteresis in the material, as well as the strains and forces output by the transducer under conditions typical of engineering applications.

Keywords: Magnetostriction, rare earth-iron alloys, Terfenol-D, magnetomechanical model, transducers

1 Introduction

We address the modeling of the magnetomechanical behavior of transducer systems which utilize magnetostrictive materials to drive structural loads. The growing interest in magnetostrictive transducers arises from the availability of highly capable magnetostrictive materials, such as the rare earth-iron alloys, which deliver strains in the 10^{-3} range and forces in the order of several KN. While magnetostrictive transducers provide adequate performance at the low signal levels where their behavior is quasilinear, the demand for high performance transducers often dictates that they be driven at the high operating regimes where hysteresis and nonlinearities are intrinsic to magnetostrictive behavior. In addition, the advantages of magnetostrictive materials over alternative transducer technologies are typically realized at high operating regimes. This motivates the development of models that accurately characterize the hysteresis and nonlinearities intrinsic to magnetostrictive transduction.

Due to the reciprocal nature of magnetomechanical transduction, magnetostrictive transducers are capable of providing not only actuation but sensing capabilities as well. One crucial aspect of the bidirectional energy exchange between the magnetic and elastic regimes is that neither transduction mechanism occurs independently, but rather they both occur simultaneously during transducer operation. In the direct or magnetostrictive effect, the action of a magnetic field and ensuing magnetization generates strains in the magnetostrictive material. These strains are in turn associated with a stress field which affects the magnetic state by virtue of the inverse or magnetomechanical effect. This issue motivates the development of models capable of addressing the magnetomechanical coupling effects intrinsic to magnetostrictive transduction.

The close connection between magnetostriction and the magnetic behavior under stress has long been recognized, and extensive experimental evidence on the magnetomechanical effect has been documented [1-3]. In recent years there has been renewed interest on this phenomenon [4, 5] because of its relevance for applications such as non-destructive evaluation and sensing. In the specific case of the R-Fe_2 (R = Tb, Dy, Sm, Ho) alloys, of which Terfenol-D ($Tb_{0.3}Dy_{0.7}Fe_{1.9-2}$) is at present the most widely known commercially available example, it has been demonstrated that desirable properties such as high magnetostriction and low hysteresis are strongly dependent upon the operating stress [6-8].

Material models such as the linear piezomagnetic equations and related formulations [9, 10] are widely used to characterize magnetostrictive transducer performance. The most common formulation for these equations is

$$\varepsilon = s^H \sigma + d_{33} H \tag{1}$$

$$B = d^*_{33} \sigma + \mu^\sigma H, \tag{2}$$

in which ε is the strain, s^H is the compliance at constant field H, d_{33} and d^*_{33} are the magnetoelastic coupling coefficients, σ is the stress, and μ^σ is the permeability at constant stress. It is emphasized that this model is in essence a generalization of two phenomenological relationships, namely the Hooke's law for linearly elastic solids $\varepsilon = s\,\sigma$ and the magnetic constitutive equation $B = \mu\, H$. The total magnetoelastic strain ε given by equation (1) is interpreted as the superposition of the elastic or passive response $\varepsilon \equiv s\,\sigma$ and the magnetostrictive component $\lambda \equiv d_{33}\, H$ associated with domain processes in the material. In a similar fashion, the magnetic induction B of equation (2) is interpreted as due to the constant-stress magnetic component $\mu^\sigma\, H$, and a term due to magnetoelastic interactions $d^*_{33}\, \sigma$. It is often assumed on the basis of small reversible magnetostrictions that $d^*_{33} = d_{33}$, which suggests that, for reversible processes, a large magnetomechanical effect $d^*_{33} \equiv (\partial B \,/\, \partial \sigma)_H$ should be observed in materials with large axial strain coefficient $d_{33} \equiv (\partial \varepsilon \,/\, \partial H)_\sigma$.

The linear piezomagnetic model provides adequate characterization of magnetostrictive performance at the low operating regimes where the behavior is quasilinear and magnetic hysteresis is negligible. At high operating regimes, however, several mechanisms lead to hysteresis, nonlinearities, and magnetoelastic coupling. These mechanisms cannot be neglected in accurate transducer models.

This paper presents a nonlinear and hysteretic magnetomechanical model for the strains and forces generated by magnetostrictive transducers in response to applied magnetic fields. The formulation presented here extends prior modeling capabilities [11, 12], which include magnetic hysteresis and nonlinearities as well as structural vibrations, by including the sensing or magnetomechanical effect in a magnetostrictive rod as it drives a transducer. This novel modeling approach provides an improved representation of the magnetomechanical behavior of magnetostrictive transducers as used in structural applications, and it provides the framework necessary for the modeling of magnetostrictive materials when utilized as sensors. The model is illustrated in the context of the prototypical Terfenol-D transducer depicted in Figure 1, but is not limited to this material or transducer design. This design provides a template for the key physical components required to fully utilize the magnetostrictive transducer capabilities, namely the magnetostrictive rod, DC magnetic circuit, AC magnetic circuit, and mechanical prestress mechanism.

The model is presented in three stages. In the first stage, discussed in Section 2, we consider the magnetization of the magnetostrictive rod under an externally applied magnetic field H and a stress field σ. The field-induced component of magnetization is quantified with the mean field model of ferromagnetic hysteresis originally developed by Jiles and Atherton [11-13]. The stress-induced component of magnetization is modeled with a law of approach to the anhysteretic magnetization as presented in [5]. The two components considered together provide a magnetization model based on the energy dissipated when domain walls attach to and unattach from inclusions in the material. Increasing magnetic fields augment the energy dissipation and hence the amount of energy lost to hysteresis. Conversely, increased stresses help to overcome domain wall pinning and hence to reduce hysteresis.

The second stage, illustrated in Section 3, involves the characterization of the magnetostriction λ produced when the magnetostrictive rod is magnetized. This is done through a phenomenological model consisting of an even-terms series expansion. While λ includes the active contribution to the strain arising from the rotation of magnetic moments, it does not account for the passive or material response of the kind found in ordinary (i.e., nonmagnetostrictive) elastic materials and modeled by $s^H \sigma$ in equation (1).

The passive effects are provided in Section 4 through consideration of force balancing in the magnetostrictive rod, in the form of a PDE equation which includes the intrinsic magnetostriction, system compliance, internal damping, and boundary conditions associated with the mechanical transducer design. The solution to this PDE provides the rod displacements and corresponding total magnetoelastic strain ε.

The complete model is summarized in Section 5, while its performance is evaluated in Section 6 by means of a comparison of model simulations with experimental measurements. Two examples are provided. In the first, the accuracy of the magnetization and strain simulations is demonstrated at two current levels and two prestress levels for a transducer designed following the guidelines of Figure 1. The second example demonstrates the ability of the model to accurately characterize the force output by a magnetostrictive rod operated under mechanically blocked conditions ($\varepsilon = 0$).

2 Magnetization of Magnetostrictive Element

Highly magnetostrictive materials such as Terfenol-D exhibit substantial deformations when magnetized. Changes in magnetization are due to the application of magnetic fields, stresses, or thermal energy. At this stage, we focus on changes in magnetization and subsequent strains produced by the application of magnetic fields and stresses. While operating temperature has a strong influence on the performance of magnetostrictive materials [16], the model in its present formulation assumes isothermal behavior. In the presence of both an applied magnetic field H and a varying stress σ, the rate of change of magnetization

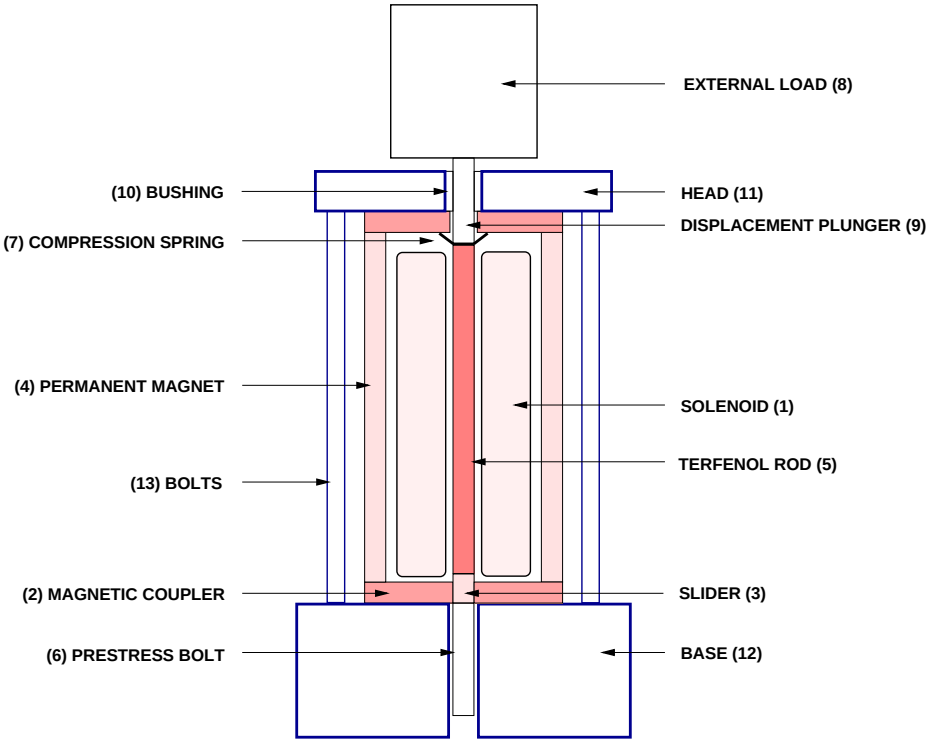

Figure 1: Cross section of the prototypical Terfenol-D transducer employed for model development.

with time $dM\,/\,dt$ is dictated by the expression

$$\frac{dM}{dt} = \left(\frac{\partial M}{\partial H}\right)\frac{dH}{dt} + \left(\frac{\partial M}{\partial \sigma}\right)\frac{d\sigma}{dt}, \tag{3}$$

which motivates treating each magnetization term independently. In the first term, the main magnetoelastic component is the differential susceptibility $\partial M\,/\,\partial H$, which is identified from the ferromagnetic hysteresis model. The time rate of change of magnetic field $dH\,/\,dt$ is readily determined since the magnetic field input to the transducer is, to a first approximation, known in advance. In the second term, it is necessary to quantify both the magnetomechanical effect $\partial M\,/\,\partial \sigma$ and the time rate of change of stress $d\sigma\,/\,dt$, since the stress depends on the amount of strain generated by the transducer.

2.1 Field-induced magnetization: differential susceptibility

The magnetization of a ferromagnetic material in response to applied magnetic fields can be explained by considering two related mechanisms [15-18]. The first mechanism is that domain walls (the transition layers between highly aligned regions termed magnetic domains) move under the influence of the magnetic field in such a way that favorably oriented domains grow at the expense of unfavorably oriented domains. The wall thickness is determined by a balance between the anisotropy, which tends to make the walls thinner, and the Weiss-type interaction coupling between atomic magnetic moments, which tends to make the walls thicker. The second mechanism involves the rotation of magnetic moments within domains towards the field direction.

In the theory originally proposed by Jiles and Atherton [11-13,19] and implemented here, the magnetization is quantified from the difference between the total magnetic energy available to magnetize the material and the energy lost to domain wall pinning. The former energy state is achieved in the anhysteretic condition, which has a magnetization value M_{an}. The energy lost to pinning is modeled assuming a friction-type

mechanism which opposes changes in magnetization. To quantify these energies, minimization of a suitable thermodynamic potential A is used to identify first the effective field H_e acting on the material,

$$H_e = H + \alpha\, M + H_\sigma, \tag{4}$$

where H is the applied field, $\alpha\, M$ is the Weiss interaction field responsible for the alignment of neighboring magnetic moments within domains, and $H_\sigma \equiv 1/\mu_0 \left[\partial \left(\frac{3}{2}\,\sigma\,\varepsilon\right)/\partial M\right]$ is the field due to magnetoelastic interactions.

The effective field calculated from expression (4) is then used to compute the anhysteretic magnetization, which is quantified using the Langevin function $\mathcal{L}(z) \equiv \coth(z) - 1/z$, with $-1 < \mathcal{L}(z) < 1$,

$$M_{an} = M_s\, \mathcal{L}(He/a), \tag{5}$$

in which M_s is the saturation magnetization and the constant a, representing the effective domain density, is treated as a parameter to be estimated through a least squares fit to the data. It is emphasized that while the Langevin function provides satisfactory fits of the ferromagnetic anhysteretic magnetization, its applicability to ferromagnets should be considered as semi-phenomenological in nature. The Langevin function was originally developed for the paramagnetic state, in which all possible orientations have the same probability and the material can be considered isotropic. In addition to being intrinsically anisotropic, the motion of domain walls in ferromagnetic materials is impeded by imperfections or pinning sites. These pinning sites, which are attributable to crystallographic defects and to the presence of dendritic twin boundaries in the case of Terfenol-D, form energy wells that are energetically favorable for domain wall attachment.

The effect of pinning sites on domain wall motion under constant stress conditions has been assessed through consideration of reversible M_{rev} and irreversible M_{irr} components of the magnetization. For low magnetic field intensities about an equilibrium level, the domain walls bend reversibly while remaining attached to pinning sites. As the applied magnetic field is increased, the domain walls achieve sufficient energy to break free from pinning sites while moving up the energy well where they were originally located, and attach to remote sites where the energy configuration is favorable. The energy lost to domain wall pinning manifests itself as hysteresis in the magnetization. This means that under the assumption of no other loss mechanisms, the hysteresis loss per unit volume and per cycle can be quantified experimentally from the area enclosed by the M-H loop.

Energy balancing is used to derive a differential equation for irreversible changes in magnetization, which can be shown to be [15]

$$M_{irr} = M_{an} - k\,\delta\,\frac{\partial M_{irr}}{\partial H_e} \tag{6}$$

where the constant k quantifies the energy needed to break pinning sites, and δ has the value +1 when $dH\,/\,dt > 0$ and -1 when $dH\,/\,dt < 0$ to ensure that the energy lost to pinning always opposes magnetization changes. Applying the chain rule, expression (6) can be modified to give the differential irreversible susceptibility,

$$\frac{\partial M_{irr}}{\partial H} = \frac{M_{an} - M_{irr}}{\delta\, k}\,\frac{\partial H_e}{\partial H}. \tag{7}$$

Recognizing that in this case the effective field given by equation (4) should be defined in terms of the irreversible magnetization,

$$H_e = H + \alpha\, M_{irr} + \frac{3}{2\,\mu_0}\,\frac{\partial\,(\sigma\,\varepsilon)}{\partial M_{irr}},$$

the partial derivative of the effective field with respect to field takes the form

$$\frac{\partial H_e}{\partial H} = 1 + \widetilde{\alpha}(M_{irr}, \sigma)\, \frac{\partial M_{irr}}{\partial H}, \tag{8}$$

where $\widetilde{\alpha}(M_{irr}, \sigma)$ is an unitless effective coupling term which is defined as

$$\widetilde{\alpha}(M_{irr}, \sigma) = \alpha + \frac{3}{2\,\mu_0}\, \frac{\partial^2(\sigma\,\varepsilon)}{\partial M_{irr}^2}.$$

It is noted that the final form of $\widetilde{\alpha}$ depends upon the characterization of ε and σ.

Direct substitution of (8) into (7) yields the differential equation for the irreversible susceptibility,

$$\frac{\partial M_{irr}}{\partial H} = \frac{M_{an} - M_{irr}}{\delta\, k - \widetilde{\alpha}(M_{irr}, \sigma)(M_{an} - M_{irr})}. \tag{9}$$

It is noted that equation (9) can yield nonphysical solutions when dH is reversed near saturation. Specifically, when the magnetization M_{irr} is below the anhysteretic M_{an} for increasing field, or when the magnetization M_{irr} is above the anhysteretic M_{an} for decreasing field, direct solution of (7) leads to a negative, and hence nonphysical, differential susceptibility. A mathematical strategy has been devised in [22] that produces a more physically consistent expression

$$\frac{\partial M_{irr}}{\partial H} = \zeta\, \frac{M_{an} - M_{irr}}{\delta\, k - \widetilde{\alpha}(M_{irr}, \sigma)(M_{an} - M_{irr})} \tag{10}$$

where

$$\zeta = \begin{cases} 1, & \{dH\,/\,dt > 0 \text{ and } M > M_{an}\} \text{ or } \{dH\,/\,dt < 0 \text{ and } M < M_{an}\} \\ 0, & \text{otherwise.} \end{cases}$$

Numerical integration of differential equation (10) gives the irreversible magnetization M_{irr}.

It has been hypothesized in [15] that the reversible component of magnetization reduces the difference between the prevailing irreversible magnetization M_{irr} and the anhysteretic magnetization M_{an} at the same field. This can be modeled mathematically with the expression

$$M_{rev} = c\,(M_{an} - M_{irr}), \tag{11}$$

where the coefficient of proportionality c quantifies the amount of reversible domain wall bulging. The value of c is determined experimentally from the ratio of the initial and anhysteretic susceptibilities [22] or through a fit to experimental data. Differentiation of equation (11) gives the reversible differential susceptibility

$$\frac{\partial M_{rev}}{\partial H} = c\, \left(\frac{\partial M_{an}}{\partial H} - \frac{\partial M_{irr}}{\partial H} \right). \tag{12}$$

Finally, the irreversible and reversible terms given by expressions (10) and (12), are added to give the total susceptibility

$$\frac{\partial M}{\partial H} = (1 - c)\, \zeta\, \frac{M_{an} - M_{irr}}{\delta\, k - \widetilde{\alpha}(M_{irr}, \sigma)\, (M_{an} - M_{irr})} + c\, \frac{\partial M_{an}}{\partial H}, \tag{13}$$

which after numerical integration gives the total magnetization arising from the application of a magnetic field. Alternatively, M can be computed by solving equation (10) and then adding M_{rev} from equation (11).

2.2 Stress-induced magnetization changes: magnetomechanical effect

We now consider the contribution of stress to the total magnetization, or magnetomechanical effect $\partial M / \partial \sigma$. A unifying description of the changes in magnetization due to the action of stress has been recently developed [4, 5, 13]. In the theory presented by Jiles [5, 14] and implemented here, the main mechanism governing the magnetomechanical effect is the unpinning of domain walls produced when a stress is applied. On the basis of the key model assumption that hysteresis is originated mainly from domain wall pinning, the freeing of domain walls from their pinning sites must cause the magnetization to change in such a way as to approach the anhysteretic.

Experimental measurements reported in [3, 4, 14, 23] clearly indicate that both the magnitude and direction of stress-induced magnetization changes are profoundly influenced by the magnetic history of the specimen. To illustrate, Figure 2 shows a schematic representation of the approach to the anhysteretic. The sample was first magnetized to saturation, and the field was then removed so that the magnetization lies close to positive or negative remanence, as respectively denoted by points A and B in Figure 2(a). The magnetization changes ΔM were then computed for varying compressive stresses while the field was held constant. The magnetization changes are illustrated in Figure 2(b). It is noted that the magnitude and direction of ΔM depend on whether the initial magnetization lies above or below the anhysteretic. Furthermore, the magnetization at point X changes slightly upon removal of the stress.

The change in magnetization exhibited by point X upon removal of the stress is explained by a second, related effect, that is the anhysteretic curve itself varies under the action of stress. Application of tensile stress to a material with positive magnetostriction coefficient (such as Terfenol-D) produces an increase in both the slope of the M-H loop and the remanent magnetization value, while compressive stress produces a shearing of the M-H loop. This effect is illustrated in Figure 3, where the influence of stress on both the anhysteretic and total magnetization is shown for the stress levels +10, 0, -10 and -20 MPa.

The net result of both effects considered in combination is that a monotonically increasing stress causes the magnetization value of X to be approached in the fashion depicted in Figure 2, while the magnetization value of X itself varies as shown in Figure 3. The magnetomechanical effect model utilized here is then formulated in the context of: (i) the effect of stress on the anhysteretic magnetization and (ii) a law of approach to the anhysteretic magnetization upon application of stress.

2.2.1 Anhysteretic Magnetization

The anhysteretic magnetization M_{an} given by expression (5) should be interpreted as a local function of both H and the particular value of the prevailing magnetization M, with both operating through the effective field H_e given by (4). For instance, at point A in Figure 4, the material is in a state of equilibrium in the presence of zero applied field, due to the coupling between magnetic moments αM and the magnetoelastic interactions H_σ in the material. Application of a small magnetic field perturbs this equilibrium slightly, giving a new value of M_{an}. Applying small field increments successively, the two-valued local anhysteretic curve shown in Figure 4 is obtained. Note, however, that global equilibrium is never achieved in this case.

A closer look at the Langevin function (5) reveals that it is possible to find a solution $\overline{M}_{an}$ which, for a given value of H and σ, satisfies the equation identically,

$$\overline{M}_{an} = M_s \, \mathcal{L}[He(\overline{M}_{an})/a]. \tag{14}$$

The solution $\overline{M}_{an}$ to the Langevin function is unique, and may be interpreted as a state of equilibrium associated with the minimization of the total energy. In consequence, the locus of points obtained by mapping all possible values of H for a given stress state is a single-valued function, as illustrated in Figure 4. We term this function the 'global' anhysteretic magnetization. The global anhysteretic $\overline{M}_{an}$

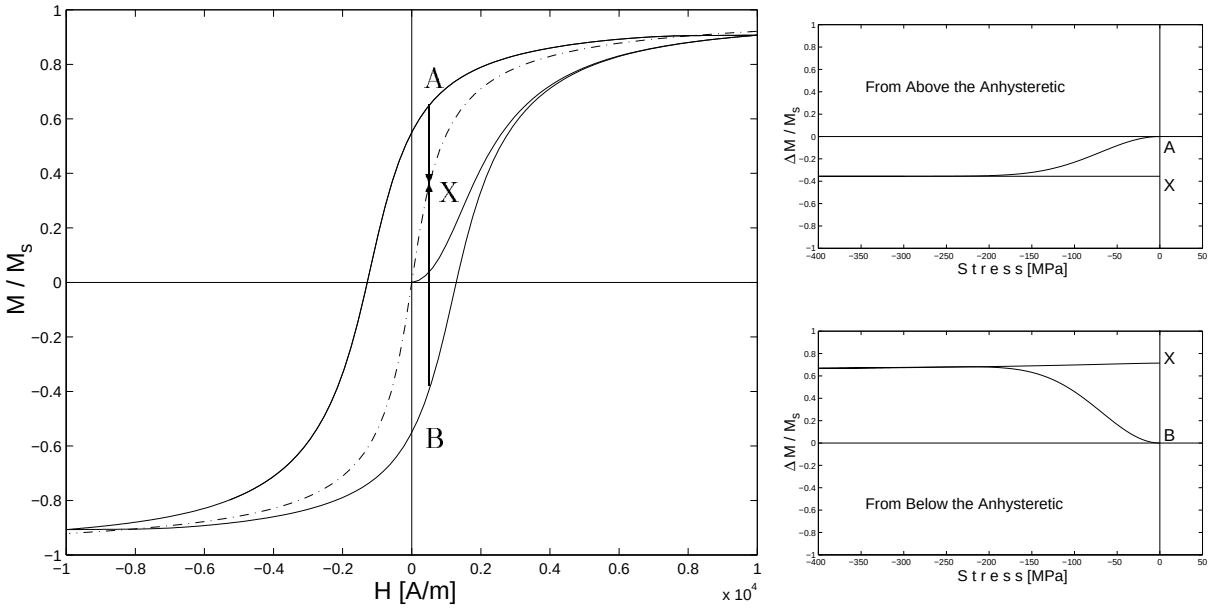

(a) (b)

Figure 2: Representation of the approach to the anhysteretic under stress, after [4]; —— total magnetization, – · – anhysteretic magnetization. (a) Arrows indicate approach in the M-H plane from positions A and B above and below the anhysteretic, for fixed H. In either case, M moves towards point X on the anhysteretic curve. (b) Trajectory of magnetization change $\Delta M/M_s$ upon application and further removal of a compressive stress, starting at point A (A $\rightarrow$ X), and at point B (B $\rightarrow$ X).

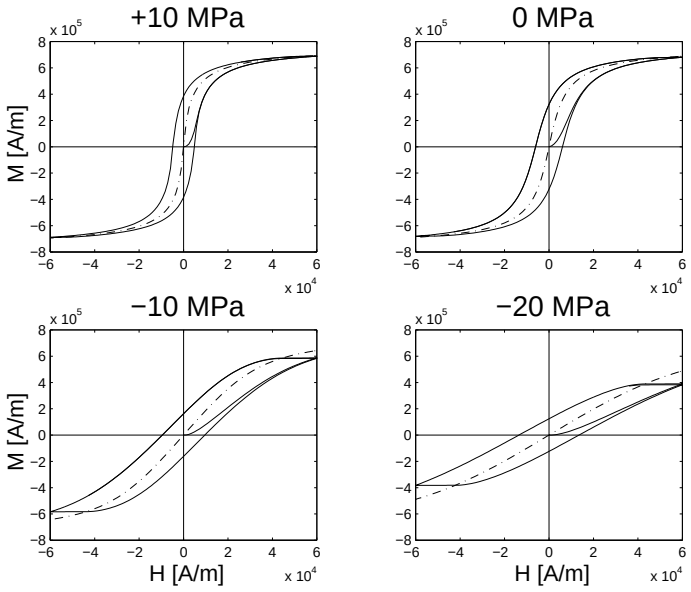

Figure 3: Model simulations representing the effect of stress on the total magnetization (——), and on the global anhysteretic magnetization (– · –), for +10, 0, -10, and -20 MPa. A positive magnetostriction coefficient is assumed [14].

is the anhysteretic used to describe the law of approach, on the basis of the observation [4] that the application of stress causes the prevailing magnetization to approach the single-valued anhysteretic state obtained in experiments by superimposing a decaying AC field on top of a fixed DC field. It is noted that in the absence of magnetic coupling ($\alpha = 0$) and constant magnetoelastic interactions ($H_\sigma \neq H_\sigma(M)$), the local and global anhysteretic curves coincide.

The global anhysteretic depends significantly on the stress state in the material. It has been even suggested [24] that the global anhysteretic defines not a curve, but a surface dependent on H and σ. This dual dependency is described in terms of the effective field H_e, by recognizing [5] that the global anhysteretic magnetization under a field H and stress σ is equivalent to the global anhysteretic magnetization under field H_e and zero stress, $\overline{M}_{an}(H,\sigma) = \overline{M}_{an}(H_e, 0)$.

In order to compute the global anhysteretic, the effective field given in equation (4) is written in the form

$$H_e = H + \overline{\alpha}(M,\sigma)\, M,$$

where the effective coupling parameter $\overline{\alpha}(M,\sigma)$ is

$$\overline{\alpha}(M,\sigma) = \alpha + \frac{3}{2\,\mu_0}\,\frac{1}{M}\,\frac{\partial(\sigma\,\varepsilon)}{\partial M}.$$

The global anhysteretic is then given by the following expression,

$$\overline{M}_{an} = M_s\,\left[\coth\left(\frac{H + \overline{\alpha}(\overline{M}_{an},\sigma)\,\overline{M}_{an}}{a}\right) - \left(\frac{a}{H + \overline{\alpha}(\overline{M}_{an},\sigma)\,\overline{M}_{an}}\right)\right],$$

which may be solved numerically using an iterative technique such as the Newton-Raphson method.

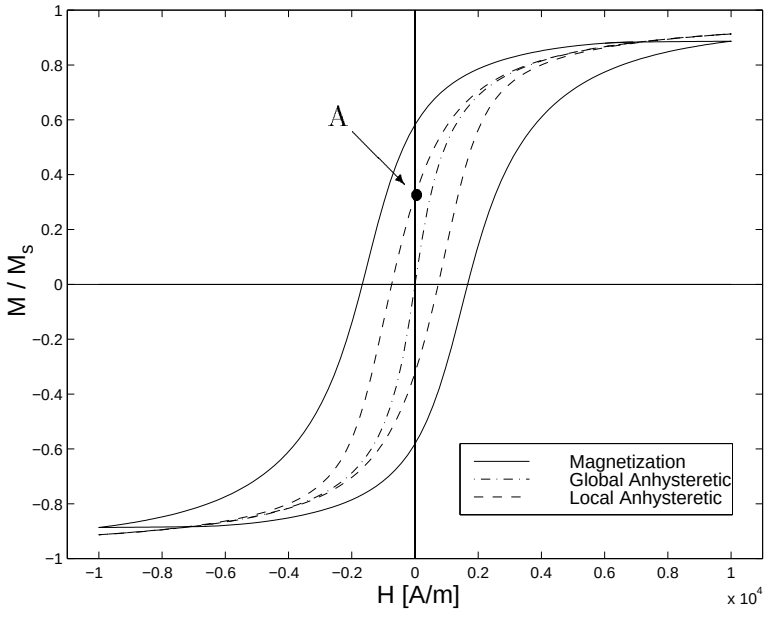

Figure 4: Model simulations showing the relative magnetization M/M_s, relative local anhysteretic $M_{an}(H,M,\sigma)/M_s = \coth[(H + \widetilde{\alpha}(M,\sigma)M)/a] - [a/(H + \widetilde{\alpha}(M,\sigma)M)]$, and relative global anhysteretic $\overline{M}_{an}(H,\sigma)/M_s = \coth[(H + \overline{\alpha}(\overline{M}_{an},\sigma)\overline{M}_{an})/a] - [a/(H + \overline{\alpha}(\overline{M}_{an},\sigma)\overline{M}_{an})]$, as a function of H.

2.2.2 Law of approach

It has been observed experimentally that the direction in which the magnetization changes with applied stress is independent of the sign of the stress, for small stresses and when the magnetization is sufficiently distant from the anhysteretic. It is then inferred that the direction of change is dependent not on the stress itself, but on a quantity which is independent of the sign of the stress. In this context, Jiles hypothesized [5] that this quantity is the elastic energy per unit volume, $W = \sigma^2/(2E)$, which is clearly independent of the sign of σ. The 'law of approach' to the anhysteretic condition is then formulated as follows: the rate of change of magnetization with elastic energy is proportional to the displacement of the prevailing magnetization from the global anhysteretic magnetization. The concept of the law of approach is now applied to the stress-induced magnetization of a magnetostrictive material.

As before, this may be posed via irreversible and reversible components of the magnetization. It is noted that to a first approximation, the application of stress produces irreversible magnetization changes since ΔM arising from stress unloading is negligible. Thus, it is reasonable to formulate the law of approach in terms of the irreversible magnetization M_{irr},

$$\frac{\partial M_{irr}}{\partial W} = \frac{1}{\xi}\left(\overline{M}_{an} - M_{irr}\right), \tag{15}$$

where ξ is a coefficient with dimensions of energy per unit volume that needs to be identified for magnetostrictive materials. Making the substitution $\partial W \,/\, \partial \sigma = \sigma /\, E$ in (15), along with application of the chain rule, permits writing the irreversible component of the magnetomechanical effect as follows,

$$\frac{\partial M_{irr}}{\partial \sigma} = \frac{\sigma}{E\,\xi}\left(\overline{M}_{an} - M_{irr}\right). \tag{16}$$

A similar argument to that used in the field-induced case yields an expression for the reversible component,

$$\frac{\partial M_{rev}}{\partial \sigma} = c\left(\frac{\partial \overline{M}_{an}}{\partial \sigma} - \frac{\partial M_{irr}}{\partial \sigma}\right), \tag{17}$$

with c the same coefficient as that defined in equation (11) because the energy available for domain wall bulging should be independent of the mechanism that produces the bulging, which can be either field- or stress-induced.

Summing the irreversible and reversible contributions leads to

$$\frac{\partial M}{\partial \sigma} = (1-c)\,\frac{\sigma}{E\,\xi}\left(\overline{M}_{an} - M_{irr}\right) + c\,\frac{\partial \overline{M}_{an}}{\partial \sigma}, \tag{18}$$

which after numerical integration gives the magnetization arising from the application of stress. As before, M may be alternatively computed by solving M_{irr} from equation (16) and then adding M_{rev} from equation (17).

3 Active Component of Strain

It is ultimately necessary to quantify the strains generated by the magnetostrictive material when a magnetic field is applied. For this purpose, we consider first the deformations occurring in the crystal lattice when the domain configuration changes. Several models exist for quantifying these deformations, including the quadratic law for domain magnetization rotation discussed in [19, 20], energy or thermodynamic formulations [23-25], elastomagnetic models [26-30], micromagnetic theories [32], magnetization rotation

analysis [7], and empirical models [5]. At low to moderate operating levels, or when material stresses are invariant, these deformations dominate over other material elastic dynamics. Under such circumstances, it is theoretically possible to quantify the bulk magnetostriction upon knowledge of the domain configuration and the magnetostriction along easy crystallographic axes. In the case of Terfenol-D, nominal values for the latter are $\lambda_{111} = 1600 \times 10^{-6}$ and $\lambda_{100} = 90 \times 10^{-6}$, and $\lambda_s \approx 1000 \times 10^{-6}$. In practical terms, however, the domain configuration cannot be known apriori.

To motivate the approach followed in this work, we consider the particular case when the magnetic field is applied perpendicular to the axis in which the magnetic moments have been aligned by application of sufficiently large compression in the case of a polycrystalline material such as Terfenol-D, or perpendicular to the easy crystallographic axis in a single crystal with uniaxial anisotropy. In either case domain rotation is the prevailing magnetization mechanism, and the magnetostriction along the field direction is given by [19]

$$\lambda(M) = \frac{3}{2}\,\lambda_s \left(\frac{M}{M_s}\right)^2, \tag{19}$$

which predicts a quadratic relation between λ and M. Expression (19) is a single-valued functional, while extensive experimental evidence demonstrates that the λ-M relationship exhibits some degree of hysteresis. For transducer modeling purposes, it is feasible to utilize a single valued λ-M functional to model the overall shape, and to let M provide the hysteresis through the hysteretic mechanisms in M-H. This approach has proven effective in previous investigations [33].

Even though (19) is consistent with the physical phenomena occurring in the above mentioned cases, it is not sufficiently general in cases when domain wall motion is significant such as when the operating stress acting on the Terfenol-D material is not extreme. In order to provide a more general magnetostriction model, we consider a series expansion symmetric about $M = 0$,

$$\lambda(M) = \sum_{i=0}^{\infty} \gamma_i\, M^{2i},$$

in which the coefficients γ_i need to be identified from experimental data. It is noted that quadratic relation (19) is achieved for $i = 1$ with $\gamma_0 = 0$ and $\gamma_1 = (3\,\lambda_s)/(2\,M_s^2)$. For implementation purposes, we consider in this study a quartic law in which the series is truncated after $i = 2$,

$$\lambda(M) = \gamma_1\, M^2 + \gamma_2\, M^4. \tag{20}$$

Note:

A convenient method for identifying γ_1 and γ_2 is by solving simultaneously the constraints at magnetic saturation M_s and at the inflection point M_0,

$$\left\{ \begin{array}{lcl} \lambda(M_s) & \equiv & \gamma_1\, M_s^2 + \gamma_2\, M_s^4 \;=\; \dfrac{3}{2}\,\lambda_s \\ \dfrac{\partial^2 \lambda}{\partial M^2}(M_0) & \equiv & 2\,\gamma_1 + 12\,\gamma_2\, M_0^2 \;=\; 0, \end{array} \right.$$

in which $(3/2)\,\lambda_s$ is the value of the magnetostriction at saturation magnetization.

4 Passive Component and Total Strain

The magnetostriction λ given by (20) quantifies the reorientation of magnetic moments towards the direction of applied field. It was shown in [12] that this magnetostriction is analogous to the term $d_{33}H$ in

linear models, but is inherently nonlinear and hysteretic through both the magnetization M and the quartic relation between M and λ. It ignores, however, the elastic properties of the magnetostrictive material as it vibrates, as represented in the linear models by $s^H\sigma$. In this section, a PDE system is formulated which models the elastic response of the magnetostrictive material and relevant transducer components located in the load path. The input to this PDE is formulated through the magnetostriction λ, which constitutes an 'internal force' driving the vibrations of the transducer. The solution to the PDE is the longitudinal displacements $u(t,x)$ relative to the prestressed position. Additional details regarding this PDE formulation are provided in [12].

The structural dynamics are modeled through consideration of the magnetostrictive rod (5), prestress bolt (6), spring (7), and mass load (8) for the transducer in Figure 1. The prestress bolt provides a stress $\sigma_0 < 0$ by compressing the magnetostrictive rod against the spring, modeled by a linear spring k_L and dashpot c_L. The rod is assumed to have length L, cross sectional area A, and longitudinal coordinate x. The material density is ρ, the elastic modulus is E, the internal damping is c_D, and the external load is modeled by a point mass m_L. It should be noted that parameter E lies between the elastic modulus at constant H, E^H, and at constant B, E^B. Since E^H and E^B depend upon the field intensity [34], so does E. However, for simplicity E is treated as a nominal or operational material stiffness.

As detailed in [11, 12], the total stress at cross sections x in the rod is given by

$$\sigma(t,x) = E\,\frac{\partial u}{\partial x}(t,x) + c_D\,\frac{\partial^2 u}{\partial x \partial t}(t,x) - E\,\lambda(t,x) + \sigma_0, \tag{21}$$

where the terms on the right hand side represent respectively the linear elasticity at small displacements, Kelvin-Voigt damping, magnetostriction-derived stress, and prestress. Force balancing then yields the dynamic model for the longitudinal displacements and strains.

For implementation purposes, the model is formulated in weak or variational form by multiplying the strong form by test functions ϕ followed by integration throughout the length of the rod. This reduces the smoothness requirements on the finite element basis since displacements and test functions need be differentiated only once compared to the second derivatives present in the strong form. The space of test functions is $V = H^1_L(0,L) \equiv \{\phi \in H^1(0,L) \mid \phi(0) = 0\}$, so that for all $\phi(x) \in V$,

$$\begin{aligned}\int_0^L \rho\,A\,\frac{\partial^2 u}{\partial t^2}(t,x)\,\phi(x)\,dx \;\; &= \;\; -\int_0^L \left[E\,A\,\frac{\partial u}{\partial x}(t,x) + c_D\,A\,\frac{\partial^2 u}{\partial x \partial t}(t,x) - E\,A\,\lambda(t,x)\right]\frac{\partial \phi}{\partial x}(x)\,dx \\ &\quad - \left[k_L\,u(t,L) + c_L\,\frac{\partial u}{\partial t}(t,L) + m_L\,\frac{\partial^2 u}{\partial t^2}(t,L)\right]\phi(L).\end{aligned} \tag{22}$$

The solution $u(t,x)$ to expression (22) defines the longitudinal displacements about the prestressed position. Once the displacements are computed, the strains are evaluated by taking derivatives with respect to position, $\varepsilon(t,x) = \partial u\,/\,\partial x(t,x)$, and the material stresses $\sigma(t,x)$ are calculated directly from (21). Note that the stress at the rod end $\sigma(t,L)$ may be equivalently calculated from the boundary condition $\sigma(t,L) = \frac{1}{A}[-k_L\,u(t,L) - c_L\,\frac{\partial u}{\partial t}(t,L) - m_L\,\frac{\partial^2 u}{\partial t^2}(t,L)]$.

5 Transducer Model Summary

In the presence of both an applied magnetic field H and stress σ, the total magnetization is dictated by the superposition of the field- and stress-dependent components given by equations (13) and (18). For implementation purposes, however, we consider the alternative approach in which the irreversible magnetization $M_{irr}(t,x)$ is computed first and added to the reversible component $M_{rev}(t,x)$ to give the

total magnetization $M(t,x)$. The superposition of expressions (10) and (16) leads to the differential equation for the time rate of change of irreversible magnetization:

$$\begin{aligned}\frac{dM_{irr}}{dt}(t,x) &= \left\{\zeta \frac{M_{an}(t,x) - M_{irr}(t,x)}{\delta\, k - \widetilde{\alpha}(M_{irr},\sigma)\,[M_{an}(t,x) - M_{irr}(t,x)]}\right\} \frac{dH}{dt}(t,x) \\ &+ \left\{\frac{\sigma(t,x)}{E\,\xi}\,\left[\overline{M}_{an}(t,x) - M_{irr}(t,x)\right]\right\} \frac{d\sigma}{dt}(t,x). \end{aligned} \tag{23}$$

To characterize $dH\,/\,dt$, it is necessary to quantify first the quasistatic field $H(t,x)$ generated by the solenoid when a current $I(t)$ circulates through it. To this end, it is often assumed that $H(t) =$ (No. turns /length) $I(t)$. However, this model is only valid in the idealized situation of a lossless, infinitely long solenoid in a lossless magnetic circuit. Experimental evidence on research transducers indicates that $H = n\,I$ is highly inaccurate because it neglects solenoid end effects, demagnetizing factors, ohmic losses, and flux leakage. One possible approach consists of identifying H-I by solving numerically Ampère's law or the Biot Savart law, using for instance finite element methods. For purposes of implementing the coupled magnetomechanical model, an experimental approach was followed which consisted of experimentally determining the magnetic circuit behavior via a position-dependent filter $\Psi(x)$ which accounts for the above-mentioned effects. Thus, the time and spatial dependencies of the field are formulated with the expression

$$H(t,x) = I(t)\,\Psi(x). \tag{24}$$

Upon substitution of equation (24) into (23), the final form for the rate of change of irreversible magnetization is obtained,

$$\begin{aligned}\frac{dM_{irr}}{dt}(t,x) &= \left\{\zeta \frac{M_{an}(t,x) - M_{irr}(t,x)}{\delta\, k - \widetilde{\alpha}(M_{irr},\sigma)\,[M_{an}(t,x) - M_{irr}(t,x)]}\right\} \frac{dI}{dt}(t)\,\Psi(x) \\ &+ \left\{\frac{\sigma(t,x)}{E\,\xi}\,\left[\overline{M}_{an}(t,x) - M_{irr}(t,x)\right]\right\} \frac{d\sigma}{dt}(t,x), \end{aligned} \tag{25}$$

which relates the irreversible magnetization with the current applied to the transducer and the varying stress arising during operation.

The reversible magnetization is calculated directly upon integration and subsequent superposition of equations (11) and (17),

$$M_{rev}(t,x) = c\,\left[M_{an}(t,x) + \overline{M}_{an}(t,x)\right] - c\,M_{irr}(t,x). \tag{26}$$

The total magnetization under the application of both a field and a stress is then given by

$$M(t,x) = (1-c)\,M_{irr}(t,x) + c\,\left[M_{an}(t,x) + \overline{M}_{an}(t,x)\right],$$

which includes the irreversible and reversible components given by equations (25) and (26), respectively. It should be noted that in the case of constant stress ($d\sigma\,/\,dt = 0$) or constant field ($dI\,/\,dt = 0$), the expression reduces to the individual components characterized by expressions (13) and (18).

After the magnetization $M(t,x)$ arising from the application of $H(t,x)$ and $\sigma(t,x)$ has been identified, the active component of strain is computed from equation (20),

$$\lambda[M(t,x)] = \gamma_1\,M^2(t,x) + \gamma_2\,M^4(t,x),$$

where it is noted that since λ depends on the applied magnetic field, it is not homogeneous throughout the rod. Hence, the magnetostriction varies along x.

The longitudinal rod displacements $u(t,x)$ are computed by solving equation (22)

$$\int_0^L \rho\, A\, \frac{\partial^2 u}{\partial t^2}(t,x)\phi(x)\,dx = -\int_0^L \left[E\, A\, \frac{\partial u}{\partial x}(t,x) + c_D\, A\, \frac{\partial^2 u}{\partial x \partial t}(t,x) - E\, A\, \lambda(t,x)\right] \frac{\partial \phi}{\partial x}(x)\,dx$$
$$- \left[k_L\, u(t,L) + c_L\, \frac{\partial u}{\partial t}(t,L) + m_L\, \frac{\partial^2 u}{\partial t^2}(t,L)\right] \phi(L).$$

To approximate the solution to this equation, a Galerkin discretization in x is used to reduce the system to a temporal system which is then solved with finite difference approximations. Details regarding the solution method used are provided in [11, 12]. Once the displacements have been characterized, the strain is computed directly using the equality

$$\varepsilon(t,x) = \frac{\partial u}{\partial x}(t,x),$$

and the corresponding stresses acting on the rod are computed directly from the strain using equation (21).

The complete elastic-magnetic coupled model is summarized in Table 1. It should be noted that for implementation purposes it is convenient to assume $\varepsilon \approx \lambda$ for computing $\widetilde{\alpha}$ and $\overline{\alpha}$, since the magnetostriction λ and its derivatives with respect to M can be formulated explicitly.

6 Model Validation

In this section, the model summarized in Table 1 is applied to two distinct example cases: (i) characterization of rod magnetization and strain output by a magnetostrictive transducer, and (ii) characterization of force generated by a magnetostrictive rod under mechanically blocked (or, equivalently, electrically short circuited) conditions.

The first example demonstrates the model accuracy for quantifying the quasistatic magnetization and strain generated by a magnetostrictive material when used in a prototypical transducer. The performance of the model is evaluated for four combinations consisting of two prestress levels and two drive current levels. It is shown that while minor changes in the coupling coefficient α and magnetostriction parameters γ_i are necessary to fine tune fits across prestress levels, a given set of parameters provides accurate fits across drive levels. The variation in α across prestress levels is explained by the fact that the anhysteretic magnetization is stress dependent, and that the shape of the anhysteretic has a strong effect on the shape of the prevailing magnetization. Regarding the magnetostriction parameters γ_i, it is noted that the domain configuration does vary when the rod is unloaded and preloaded again for operation at a new prestress value. It is then expected that these domain configuration changes be accounted for by variations of parameters γ_i.

A variety of transducer applications require high forces of the kind typically associated with mechanically blocked or near-blocked conditions. Examples of such applications include shaft clamping in inchworm-type linear motors [35], mitigation of seismic vibrations in buildings, and deep-submersion underwater communications. This motivates the evaluation of the stress calculations provided by the model. Hence, in the second example, model simulations of transducer force output are compared with experimental measurements performed under mechanically blocked conditions ($\varepsilon(t,L) = 0$). Experimental tests were performed for four different drive current levels, at a constant prestress. It is shown that a fixed set of parameters provides accurate characterization of the force produced by a magnetostrictive rod.

6.1 Example 1

The model is applied to a Terfenol-D transducer with the configuration illustrated in Figure 1 and used to characterize the quasistatic magnetization and displacement produced by the transducer in response to an

Table 1: Coupled structural-magnetic model quantifying the magnetization, strain, and stress.

Magnetic Model:

$$H(t,x) = I(t)\,\Psi(x)$$

$$\overline{\alpha}(M,\sigma) = \alpha + \frac{3}{2\,\mu_0}\,\frac{1}{M}\,\frac{\partial(\sigma\,\varepsilon)}{\partial M}$$

$$M_{an}(t,x) = M_s\,\left[\coth\left(\frac{H(t,x)+\overline{\alpha}(M,\sigma)\,M(t,x)}{a}\right) - \left(\frac{a}{H(t,x)+\overline{\alpha}(M,\sigma)\,M(t,x)}\right)\right]$$

$$\overline{M}_{an}(t,x) = M_s\,\left[\coth\left(\frac{H(t,x)+\overline{\alpha}(\overline{M}_{an},\sigma)\,\overline{M}_{an}(t,x)}{a}\right) - \left(\frac{a}{H(t,x)+\overline{\alpha}(\overline{M}_{an},\sigma)\,\overline{M}_{an}(t,x)}\right)\right]$$

$$\widetilde{\alpha}(M_{irr},\sigma) = \alpha + \frac{3}{2\,\mu_0}\,\frac{\partial^2(\sigma\,\varepsilon)}{\partial M_{irr}^2}$$

$$\begin{aligned}\frac{dM_{irr}}{dt}(t,x) &= \left\{\zeta\,\frac{M_{an}(t,x)-M_{irr}(t,x)}{\delta\,k-\widetilde{\alpha}(M_{irr},\sigma)\,[M_{an}(t,x)-M_{irr}(t,x)]}\right\}\,\frac{dI}{dt}(t)\,\Psi(x)\\ &\quad+\left\{\frac{\sigma(t,x)}{E\,\xi}\,\left[\overline{M}_{an}(t,x)-M_{irr}(t,x)\right]\right\}\frac{d\sigma}{dt}(t,x)\end{aligned}$$

$$M_{rev}(t,x) = c\,\left[M_{an}(t,x)+\overline{M}_{an}(t,x)\right] - c\,M_{irr}(t,x)$$

$$M(t,x) = (1-c)\,M_{irr}(t,x) + c\,\left[M_{an}(t,x)+\overline{M}_{an}(t,x)\right]$$

Structural Model:

$$\lambda[M(t,x)] = \gamma_1\,M^2(t,x) + \gamma_2\,M^4(t,x)$$

$$\begin{aligned}\int_0^L \rho\,A\,\frac{\partial^2 u}{\partial t^2}(t,x)\phi(x)\,dx &= -\int_0^L\left[E\,A\,\frac{\partial u}{\partial x}(t,x)+c_D\,A\,\frac{\partial^2 u}{\partial x\partial t}(t,x)-E\,A\,\lambda(t,x)\right]\,\frac{\partial\phi}{\partial x}(x)\,dx\\ &\quad-\left[k_L\,u(t,L)+c_L\,\frac{\partial u}{\partial t}(t,L)+m_L\,\frac{\partial^2 u}{\partial t^2}(t,L)\right]\,\phi(L)\end{aligned}$$

$$\varepsilon(t,x) = \frac{\partial u}{\partial x}(t,x)$$

$$\sigma(t,x) = E\,\frac{\partial u}{\partial x}(t,x) + c_D\,\frac{\partial^2 u}{\partial x\partial t}(t,x) - E\,\lambda(t,x) + \sigma_0$$

applied current $I(t)$. The measured output from the transducer during operation included driving voltage and current, voltage induced in the pickup coil, and rod displacement. The prestress levels were -6.9 and -10.35 MPa (-1.0 and -1.5 ksi), and the drive current levels were 4.0 and 16.0 A zero-pk. The operating temperature was monitored with a thermocouple and was confined to the range 21-28°C.

The driver was a 115 mm (4.53 in) long, 12.7 mm (0.5 in) diameter, monolithic $Tb_{0.3}Dy_{0.7}Fe_{1.92}$ rod manufactured using the modified Bridgman process. The magnetic field excitation $H(t)$ was provided by a surrounding solenoid, while an innermost one-layer pickup coil was used to collect magnetic induction measurements. The 1 Hz excitation frequency was provided by a Tektronix 2642A Personal Fourier Analyzer connected to a Techron 7780 amplifier operating in current control mode. The magnetic induction $B(t)$ was calculated by integration of the pickup coil signal V_{pu}. Following the Faraday-Lenz law of magnetic induction, $B(t) = -1/(N_{pu}\, A_{pu}) \int_0^t V_{pu}(\tau)\, d\tau$, where A_{pu} is the mean cross sectional area of the pickup coil and N_{pu} is the number of turns in the pickup coil. The magnetization used for comparison with model simulations was computed from the magnetic constitutive equation $M = (B/\mu_0) - H$.

Flux closure was provided by 1018 steel end caps and a cylindrical Alnico V permanent magnet, which was demagnetized to obtain unbiased operation. A slider and a Belleville compression washer completed the magnetic circuit.

The compressive preloading necessary to avoid tensile stresses on the moderately brittle Terfenol-D rod was provided by a steel bolt located within the transducer base. The bolt pushed the rod against the compression washer, whose stiffness k_{mps} was calculated from the linear region of its force-displacement characteristic curve. A PCB 208A13 force transducer located between the prestress bolt and the Terfenol-D rod was used during preloading to obtain the desired preload value.

The external load was a mass threaded onto the displacement plunger which weighed $m_L = 0.5$ Kg. The load displacement (i.e., the transducer output) was measured with a Lucas Schaevitz LVM-110 linear variable differential transducer equipped with a 025-MHR probe. The corresponding bulk strain, used for comparison with model simulations, was computed by dividing this displacement by L.

For identification of the Ψ filter, a series of flux measurements was conducted with a Hall effect probe (F. W. Bell 9500 series), located within the transducer to allow characterization of end effects, demagnetizing factors, and magnetic circuit nonlinearities. A DC current was used to excite the solenoid, and the flux density $B_{sur}(x)$ was measured adjacent to the surface of the rod at locations 5 mm apart over a longitudinal line. Since in air $B = H$ in the CGS units system, the flux density is equal to the magnetic field, $B_{sur}(x) = H_{sur}(x)$. The correction functional was then computed from $\Psi(x) = H_{sur}(x) \,/\, I$. Additional details regarding the experimental analysis are provided in [11, 12].

The magnetization and strain calculations measured from the experimental transducer are shown in Figure 5. It should be noted that the reversal of strain magnitude observed across drive levels when the prestress is changed from -6.9 MPa to -10.35 MPa is consistent with the data reported in [36].

The performance of the model is illustrated in Figures 6 and 7. The model provides in all cases very accurate fits of both the measured rod magnetization and transducer strain output. It should be noted that the model does not provide a mechanism to account for the contraction observed in the magnetization data at low field levels, which explains the discrepancy observed in the 4.0 A cases. It is expected that a higher order truncation of the magnetostriction expansion should translate into improved strain fits.

6.2 Example 2

The model is now used to characterize the force output by a 19.05 mm (0.75 in) long, 8.89 mm (0.35 in) diameter, monolithic $Tb_{0.3}Dy_{0.7}Fe_{1.92}$ FSZM rod. A testing clamp was devised to maintain mechanically blocked conditions during operation, which consisted of a stainless steel base where the rod and magnetic circuit assembly were located and a stainless steel cap which housed a PCB A13 force transducer. The cap was attached to the base via stainless steel bolts, which were tightened until the desired prestress value

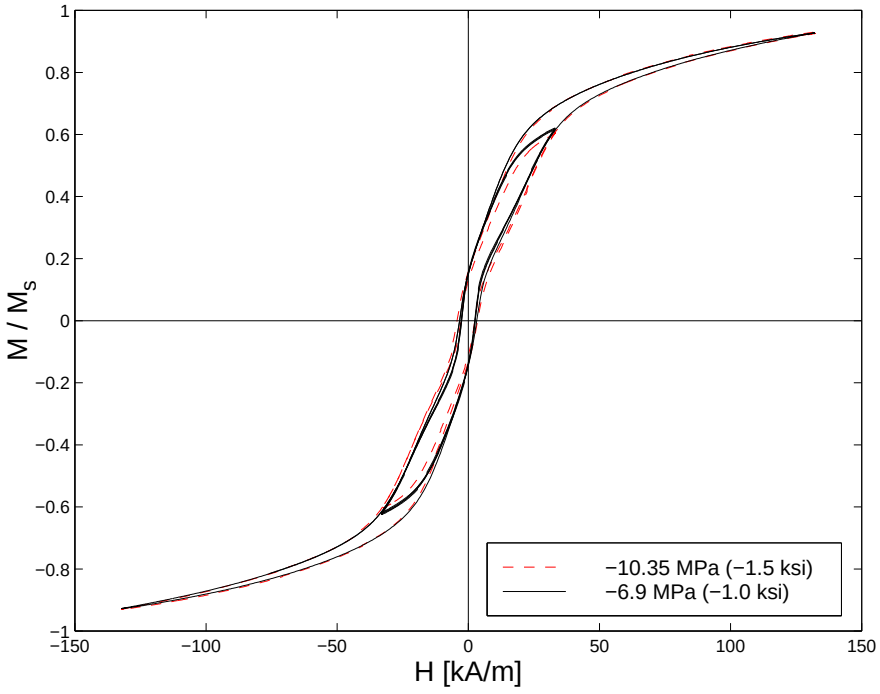

(a)

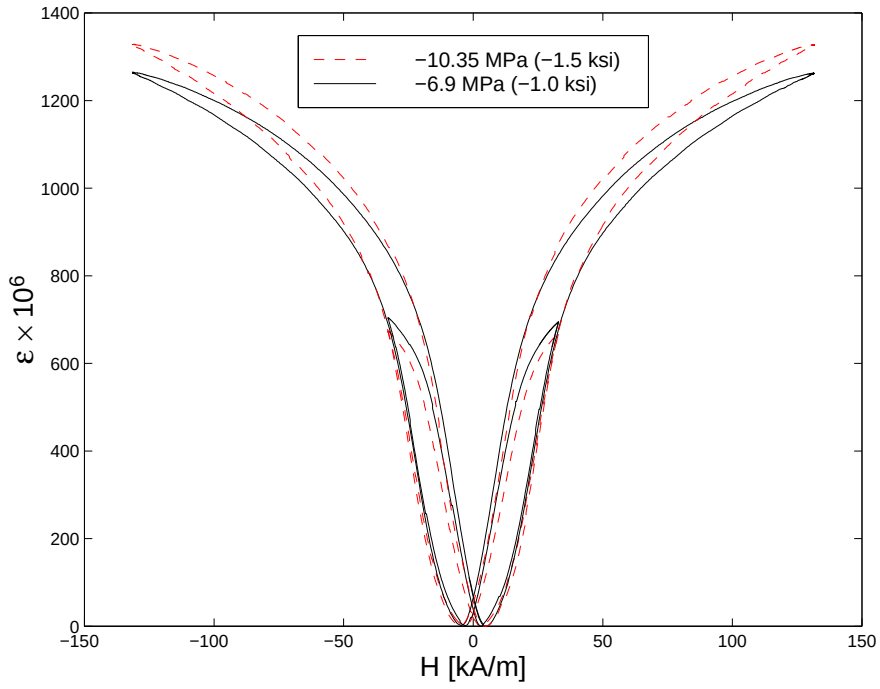

(b)

Figure 5: Experimental data collected from a Terfenol-D transducer, at the prestress values $-6.9/-10.35$ MPa and the drive current levels 4.0/16.0 A zero-pk. (a) Magnetization and (b) output strain.

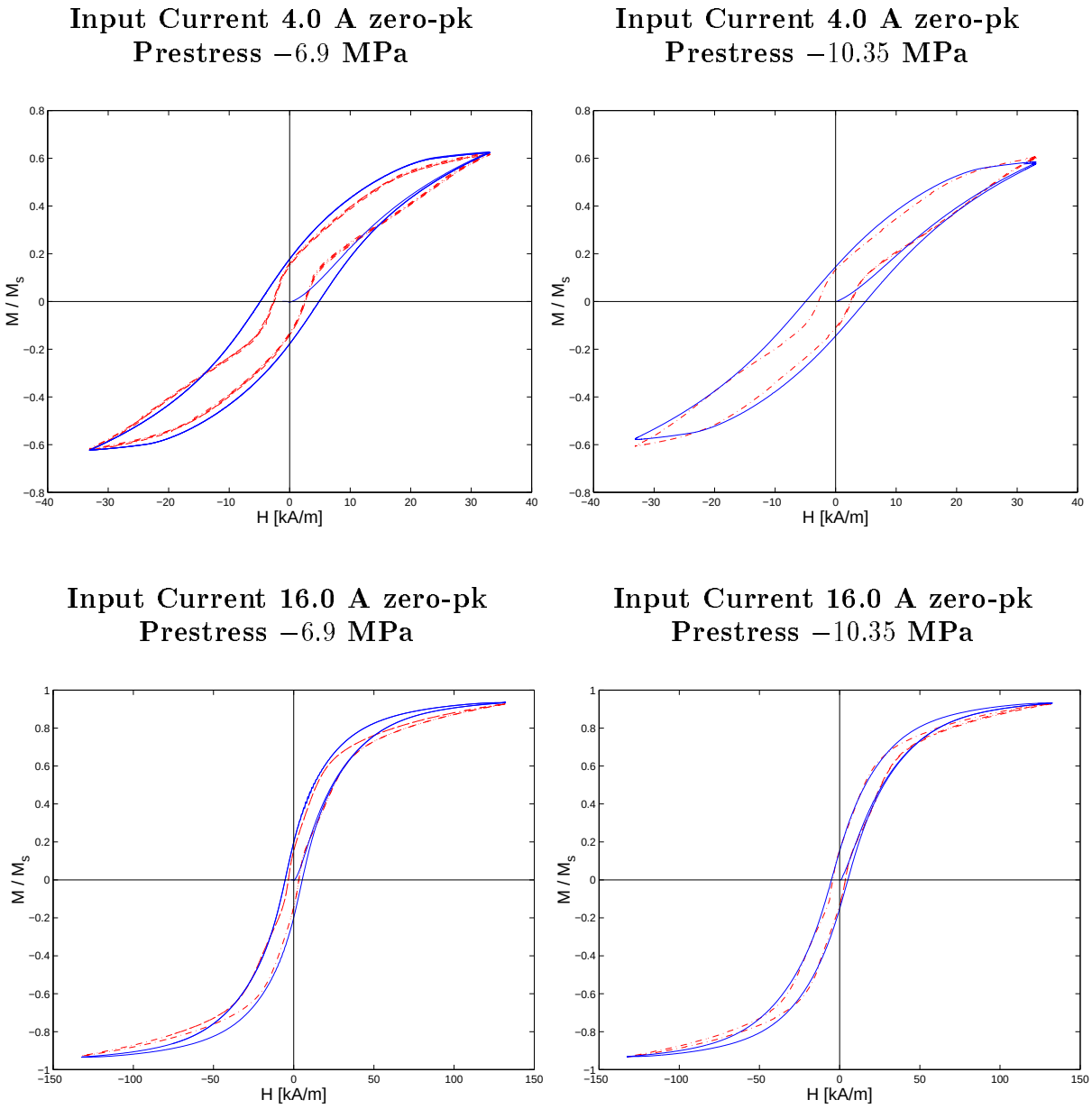

Figure 6: Magnetization results: comparison of model simulations (——) with experimental data (– · –). Constant values of the model parameters were $a = 7000$ A/m, $k = 7000$ A/m, $c = 0.2$, $\alpha = 0.045$, $E = 30$ GPa, $\rho = 9250$ Kg/m^3, $\gamma_1 = 2.95\times10^{-15}$ m^2/A^2, $\gamma_2 = -6\times10^{-28}$ m^4/A^4, $\xi = 2.45 \times 10^4$ Pa, $c_D = 1 \times 10^6$ Ns/m, $c_L = 1 \times 10^3$ Ns/m, $k_L = 2.5 \times 10^6$ N/m, $m_L = 0.5$ Kg, $L = 0.115$ m, $D = 0.0127$ m.

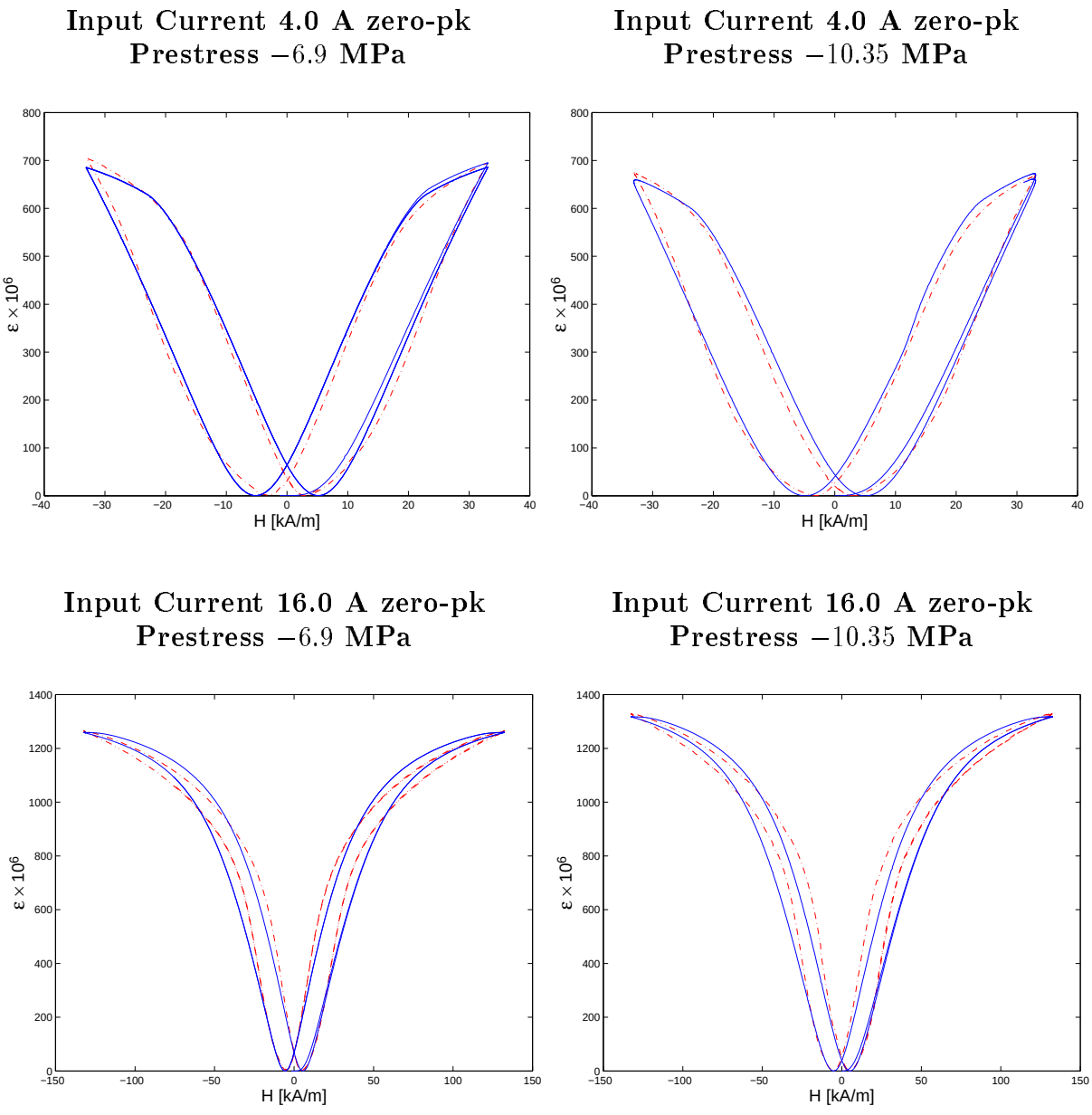

Figure 7: Strain results: comparison of model simulations (——) with experimental data (−·−). Constant values of the model parameters were same as in Figure 6.6, except $\alpha = 0.065$, $\gamma_1 = 3.12 \times 10^{-15}$ m^2/A^2.

was read from the force transducer.

The magnetic field $H(t)$ was supplied by a 400-turn solenoid, which was calibrated using a Hall effect probe in the fashion described in Example 1. The magnetic circuit was completed by two magnetic steel end pieces and a surrounding magnetic steel cylinder.

The tests were performed at a prestress value of -6.9 MPa for four drive current levels: 0.5, 1.0, 1.5, and 2.0 A zero-pk. The excitation signal was 1 Hz in all cases. The operating temperature remained in all cases between 21-30°C. The force versus magnetic field measurements are shown in Figure 8.

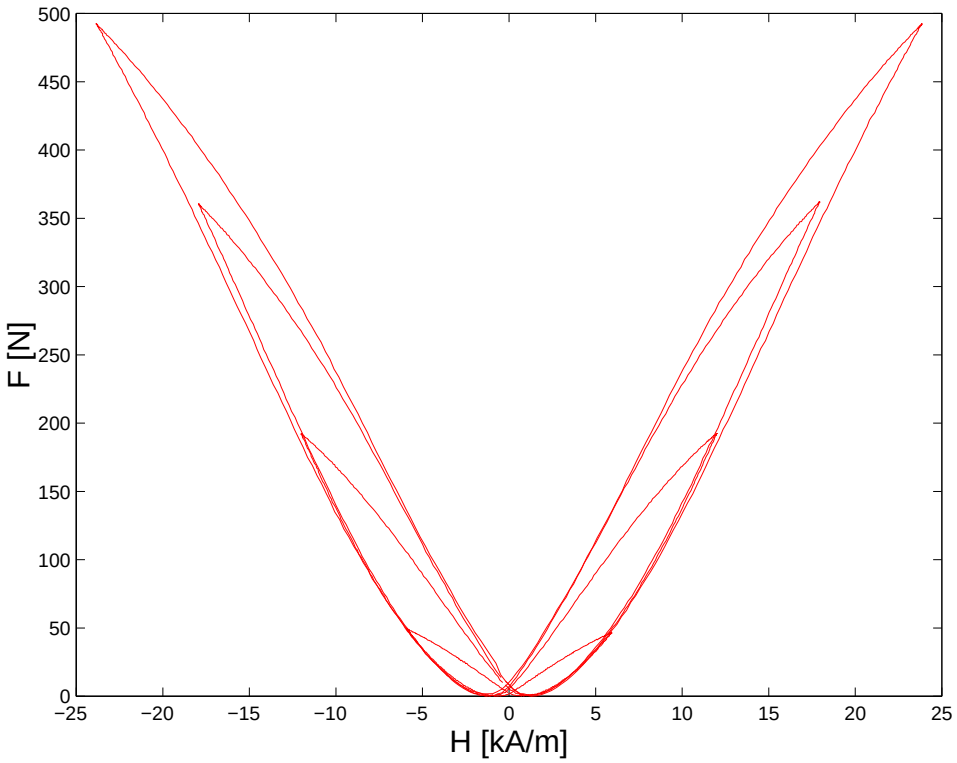

Figure 8: Force versus magnetic field generated by the Terfenol-D rod under blocked conditions, for the drive levels 0.5, 1.0, 1.5, and 2.0 A zero-pk. The prestress was $\sigma_0 = -6.9$ MPa.

Although in theory the clamp's stiffness should be infinity, the manufacturer's specifications for the force transducer were commensurate with that of the Terfenol-D rod itself. To model this condition, the specified stiffness value was assigned to the boundary spring, $k_{mps} = 1.75 \times 10^8$ N/m. In a similar fashion, the dynamic mass was weighed and assigned to the corresponding model mass load, $m_L = 5$ Kg.

It should be noted that the elastic modulus under blocked conditions (or equivalently, under constant magnetic induction conditions) represents the intrinsic material stiffness and is the largest value that the material can achieve for a given operating condition. The value of the elastic modulus used in these simulations was $E = 60$ GPa, in accordance with the experimental measurements reported in [34].

Model simulations and experimental measurements are compared in Figure 9. The model performance is extremely satisfactory at all drive levels, both in quantifying the amplitude of the force and the hysteresis present in the data. It is emphasized that the same set of values for model parameters was used in all cases.

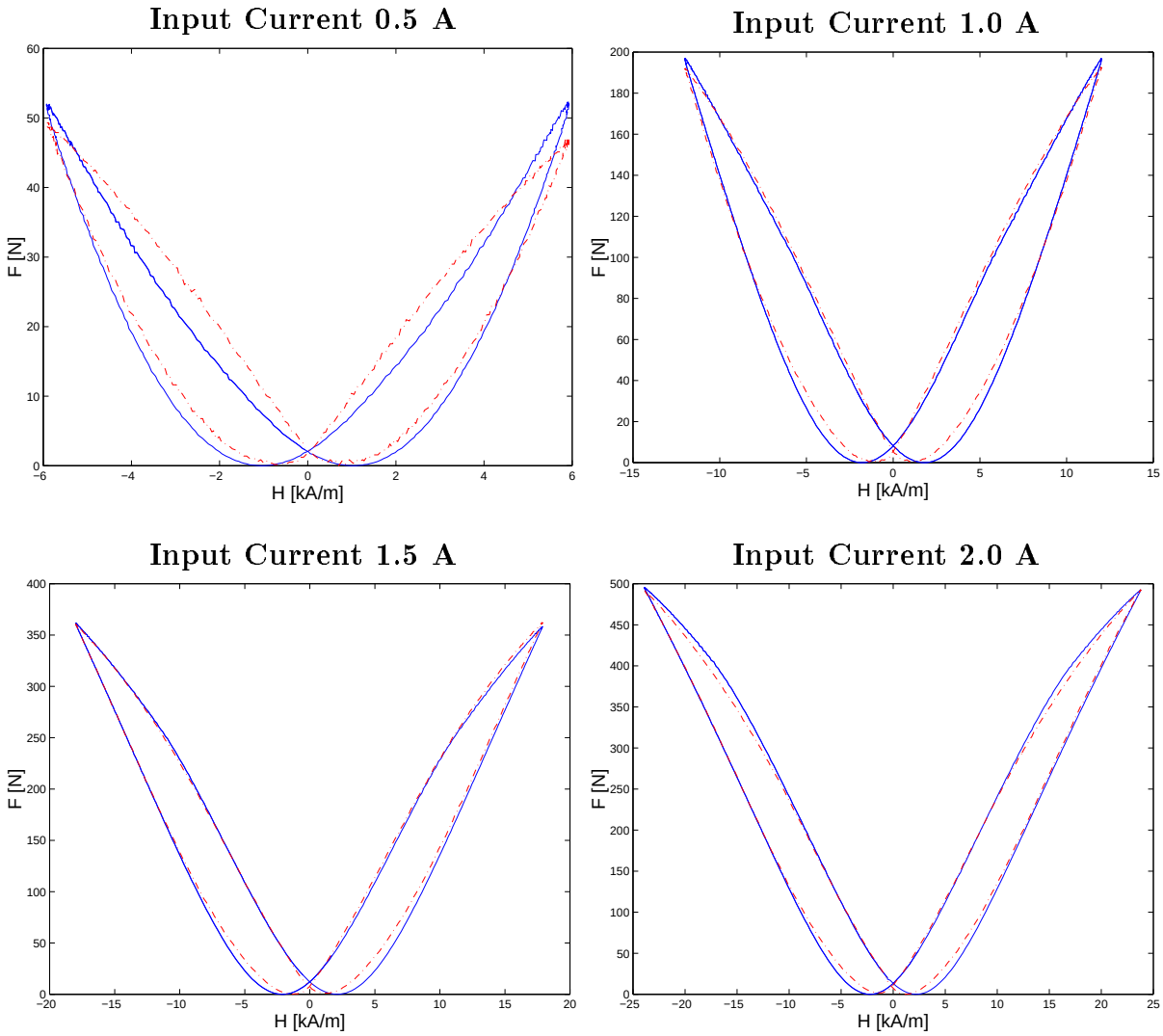

Figure 9: Comparison of model simulations (——) with experimental data (– · –) at four drive levels and prestress of $\sigma_0 = -6.9$ MPa. The constant values of the model parameters were $a = 4000$ A/m, $k = 5000$ A/m, $c = 0.4$, $\alpha = 0.001$, $E = 60$ GPa, $\rho = 9250$ Kg/m^3, $\gamma_1 = 7 \times 10^{-16}$ m^2/A^2, $\gamma_2 = -1 \times 10^{-29}$ m^4/A^4, $\xi = 2.45 \times 10^4$ Pa, $c_D = 1 \times 10^5$ Ns/m, $c_L = 1 \times 10^3$ Ns/m, $k_L = 1.75 \times 10^8$ N/m, $m_L = 5$ Kg, $L = 0.019$ m, $D = 0.009$ m.

7 Concluding Remarks

A coupled magnetomechanical model for the magnetization and strain behavior of magnetostrictive transducers in response to applied currents has been presented. The model includes the nonlinearities and hysteresis present in the magnetic response of magnetostrictive materials, and the linear elastic effects which are characteristic of high-signal magnetostrictive transduction. The magnetic and structural regimes are coupled through the magnetization, which varies in response to both the externally applied magnetic field and the stress field which arises as the transducer actuates upon an external load.

The model was constructed in three steps. In the first, the mean field theory of Jiles and Atherton was used as a basis for quantifying the relation between the current input to the transducer and the magnetization. The magnetization arising from variations in stress was also addressed, by considering a 'law of approach' to the anhysteretic magnetization. The resulting magnetization model provides a representation of the hysteresis and saturation effects taking place when domain walls attach to and unattach from pinning sites in the material. Pinning sites provide a mechanism for restraining the motion of domain walls as the field is cycled, and hence for magnetization hysteresis. The stress acting on the material produces domain wall unpinning and hence causes the magnetization to approach the anhysteretic state. In the second step, the magnetostriction due to the rotation of magnetic moments was quantified by means of a quartic model formulated in terms of the magnetization. Finally, force balancing was posed in the form of a PDE equation which includes the magnetostriction, system compliance, internal damping, and boundary conditions given by the transducer design. The solution to this PDE provides the material displacements and forces produced by the transducer.

The examples demonstrated the accuracy of the model in two cases typical of magnetostrictive transducer applications. In the first, the magnetization and strain output by a typical actuator were characterized at two drive levels and two prestress levels. A near-constant set of parameters was used across drive levels and prestresses. In the second example, the force output by a magnetostrictive rod operated under mechanically blocked conditions was characterized for four drive levels and fixed prestress. A constant set of model parameters provided accurate simulations across drive levels.

Acknowledgments

The authors wish to thank David Jiles for his helpful suggestions regarding the modeling techniques employed here. Financial support for M.J.D. and A.B.F. was provided by the NSF Young Investigator Award #CMS9457288 of the Division of Civil and Mechanical Systems. The work of R.C.S. was supported in part by the Air Force Office of Scientific Research under the grant AFOSR F49620-98-1-0180.

References

[1] W. F. Brown, "Irreversible magnetic effects of stress," *Phys. Rev.*, **75**(1):147–154, January 1949.

[2] R. M. Bozorth and H. J. Williams, "Effect of small stresses on magnetic properties," *Rev. Mod. Phys.*, **17**(1):72–80, January 1945.

[3] R. R. Birss, C. A. Faunce and E. D. Isaac, "Magnetomechanical effects in iron and iron-carbon alloys," *J. Phys. D: Appl. Phys.*, 4:1040–1048, 1971.

[4] K. C. Pitman, "The influence of stress on ferromagnetic hysteresis," *IEEE Trans. Magn.*, **26**(5), September 1990.

[5] D. C. Jiles, "Theory of the magnetomechanical effect," *J. Phys. D: Appl. Phys.*, **28**:1537–1546, 1995.

[6] M. L. Spano A. E. Clark and H. T. Savage, "Effect of stress on the magnetostriction and magnetization of rare earth-$Fe_{1.95}$ alloys," *IEEE Trans. Magn.*, **MAG-19**(5):1964–1966, September 1983.

[7] A. E. Clark, H. T. Savage and M. L. Spano, "Effect of stress on the magnetostriction and magnetization of single crystal $Tb_{0.27}Dy_{0.73}Fe_2$," *IEEE Trans. Magn.*, **MAG-20**(5), 1984.

[8] F. T. Calkins, M. J. Dapino, and A. B. Flatau, "Effect of prestress on the dynamic performance of a Terfenol-D transducer," In *Proc. of SPIE Smart Structures and Materials*, Vol. 3041, pp. 293–304, San Diego, CA, March 1997.

[9] D. L. Hall, *Dynamics and vibrations of magnetostrictive transducers*, PhD dissertation, Iowa State University, Ames, IA, 1994.

[10] T. A. Duenas, L. Hsu and G. P. Carman, "Magnetostrictive composite material systems analytical/experimental," In *Adv. Smart Materials Fundamentals an Applications*, Boston, MA, 1996.

[11] M. J. Dapino, R. C. Smith, and A. B. Flatau, "An active and structural strain model for magnetostrictive transducers," In *Proceedings of SPIE, Smart Structures and Materials 1998*, Vol. 3329, pp. 198–209, San Diego, CA, March 1998.

[12] M. J. Dapino, R. C. Smith, and A. B. Flatau, "A structural-magnetic strain model for magnetostrictive transducers," *CRSC Technical Report* CRSC-TR98-31, 1998, and submitted to *IEEE Trans. Magn.*

[13] D. C. Jiles and D. L. Atherton, "Ferromagnetic hysteresis," *IEEE Trans. Magn.*, **MAG-19**(5):2183–2185, 1983.

[14] D. C. Jiles and D. L. Atherton, "Theory of the magnetization process in ferromagnets and its application to the magnetomechanical effect," *J. Phys. D: Appl. Phys.*, **17**:1265–1281, 1984.

[15] D. C. Jiles and D. L. Atherton, "Theory of ferromagnetic hysteresis," *J. Magn. Magn. Mater.*, **61**:48–60, 1986.

[16] A. E. Clark, "High power rare earth magnetostrictive materials," In *Procs. Recent Advances in Adaptive and Sensory Materials and Their Applications*, pp. 387–397, Lancaster, PA, Technomic Publishing Co., Inc., 1992.

[17] D. C. Jiles, *Introduction to Magnetism and Magnetic Materials*, Chapman & Hall, London, First edition, 1991.

[18] R. M. Bozorth, *Ferromagnetism*, D. Van Nostrand, Inc., 1968.

[19] B. D. Cullity, *Introduction to magnetic materials*, Addison-Wesley, Reading, MA, 1972.

[20] S. Chikazumi, *Physics of magnetism*, R. E. Krieger Publishing, Malabar, FL, 1984.

[21] D. C. Jiles and D. L. Atherton, "Theory of ferromagnetic hysteresis," *J. Appl. Phys.*, **55**(6):2115–2120, 1984.

[22] D. C. Jiles, J. B. Thoelke and M. K. Devine, "Numerical determination of hysteresis parameters for the modeling of magnetic properties using the theory of ferromagnetic hysteresis," *IEEE Trans. Magn.*, **28**(1):27–35, 1992.

[23] D. J. Craik and M. J. Wood, "Magnetization changes induced by stress in a constant applied field," *J. Phys. D: Appl. Phys.*, 4:1009, 1971.

[24] M. J. Sablik and R. A. Langman, "Approach to the anhysteretic surface," *J. Appl. Phys.*, **79**(8):6134–6136, 15 April 1996.

[25] M. J. Sablik and D. C. Jiles, "Coupled magnetoelastic theory of magnetic and magnetostrictive hysteresis," *IEEE Trans. Magn.*, **29**(3), 1993.

[26] F. Delince, A. Genon, J. M. Gillard, H. Hedia, W. Legros and A. Nicolet, "Numerical computation of the magnetostriction coefficient in ferromagnetic materials," *J. Appl. Phys.*, **69**(8):5794–5796, 1991.

[27] V. Agayan, "Thermodynamic model for ideal magnetostriction," *Physica Scripta*, **54**:514–521, 1996.

[28] W. P. Mason, *Electromechanical transducers and wave filters*, D. Van Nostrand, Toronto, 1942.

[29] F. Claeyssen, R. Bossut and D. Boucher, "Modeling and characterization of the magnetostrictive coupling," In *Power Transducers for Sonics and Ultrasonics*, B. F. Hamonic, O. B. Wilson and J.-N. Decarpigny, Eds., pp. 132–151, Toulon, France, Springer-Verlag, June 1990.

[30] C. H. Sherman and J. L. Butler, "Analysis of harmonic distortion in electroacoustic transducers," *J. Acoust. Soc. Am.*, **98**(3):1596–1611, 1995.

[31] F. Claeyssen, N. Lhermet and R. L. Letty, "Design and construction of a resonant magnetostrictive motor," *IEEE Trans. Magn.*, **32**(5):4749–4751, 1996.

[32] R. D. James and D. Kinderlehrer, "Theory of magnetostriction with applications to $Tb_xDy_{1-x}Fe_2$," *Philosophical Magazine B*, **68**(2):237–274, 1993.

[33] F. T. Calkins, *Design, analysis and modeling of giant magnetostrictive transducers*, PhD dissertation, Iowa State University, Ames, Iowa, 1997.

[34] M. J. Dapino, F. T. Calkins and A. B. Flatau, "Statistical analysis of Terfenol-D material properties, In *Proceedings of SPIE, Smart Structures and Materials 1997*, Vol. 3041, pp. 256–267, San Diego, CA, March 1997.

[35] W. Chen J. Frank, G. H. Koopmann and G. A. Lesieutre, "Design and performance of a high force piezoelectric inchworm motor," In *Proc. of SPIE Smart Structures and Materials*, Newport Beach, CA, March 1999. To be published.

[36] J. L. Butler, *Application manual for the design of ETREMA Terfenol-D magnetostrictive transducers*, ETREMA Products, Inc., Ames, IA, 1988.